http://dx.doi.org/10.1109/LRA.2016.2530859

Generalized Predictive Control of a Surgical Robot for Beating-heart Surgery Under Delayed and Slowly-sampled Ultrasound Image Data

Meaghan Bowthorpe and Mahdi Tavakoli

***Abstract*—Operating on a beating heart would offer many benefits to patients. The risks associated with heart-lung machines used in arrested-heart surgery would be eliminated and the effectiveness of reconstructive procedures could be judged immediately. However, the heart's fast beating motions make operating on a beating heart impossible for the surgeon. With advances in surgical robotics, we can now envision a robot-assisted surgical system that first synchronizes the surgical robot with the beating heart motion and then lets the surgeon operate through teleoperation on a seemingly motionless point on the heart. This paper presents such a system that relies on both motion prediction and predictive control to overcome the delays introduced in acquiring the beating heart's position from ultrasound images. Also, slowly sampled position data originating from low-frame-rate ultrasound images is treated with cubic interpolation and extended Kalman filter-based prediction. The results of a user study involving a task based on mitral valve annuloplasty are presented to show the proposed method's efficacy in terms of synchronizing the surgical robot to the beating heart motion.**

***Index Terms*—Medical Robots and Systems, Surgical Robotics: Laparoscopy, Control Architectures and Programming**

I. Introduction

CURRENTLY, performing a surgical procedure on a beating heart is extremely difficult as the surgeon must manually track the heart's fast beating motion and simultaneously perform a surgical procedure. Presently, if the procedure is performed on the heart's surface, a mechanical stabilizer can locally suppress the beating motion. However, not all of the motion is eliminated [1]. Alternatively, the patient can be connected to a heart-lung bypass machine and then his/her heart is stopped. This allows the surgeon to operate on a stationary heart, but increases the patient's risk of stroke and long-term cognitive loss [2], [3]. The ability to operate on a beating heart would benefit patients as the risks associated with mechanical stabilization and arrested-heart surgery could be greatly reduced and the procedure's effectiveness could be judged immediately. This would be possible if a surgical robot is controlled to move in synchrony with a point of interest (POI) on the beating heart. Then, this point would appear stationary with respect to the surgical tool tip. The surgeon's motions would then be superimposed on the surgical robot's synchronization motions via teleoperation, and the surgeon could operate on a seemingly stationary heart.

Various configurations of such a system have been presented. Some use a mechanical stabilizer to reduce the physiological motion and then compensate for the residual motion [1]. However, the heart is not beating freely and the surgical procedure can only be performed on the heart's exterior surface. Others that allow the heart to beat freely measure the POI's motion from an external sensor. These motion sensors can be divided into three major categories: (a) force sensors, (b) position sensors such as sonomicrometry crystals, and (c) image-based sensors, such as cameras, endoscopes, and ultrasound (US) imaging. In case (a), a desired contact force is kept between the surgical tool and the POI. In cases (b) and (c), a desired distance is kept between the surgical tool and the POI.

Force-based surgical systems (case (a)) are preferable in scenarios such as ablation [4], [5], [6] or tissue palpation [7], where constant contact between the surgical instrument and the POI is required. The disadvantage is that the surgical tool and the heart tissue must always be in contact, which does not always occur in an operative setting.

An alternative is to measure the POI's and surgical tool's positions and maintain a desired distance between them. Sonomicrometry crystals sutured directly to the heart tissue can measure the POI's position (case (b)) [8], [9], [10], [11]. As the crystals are sutured onto the POI, this method is difficult to implement in the operating theatre, especially for intracardiac procedures. Also, the data processing cannot be performed in real-time [11].

Real-time position measurements can be collected from images (case (c)). High-speed cameras, with frame rates of 955 Hz and 500 Hz, have been proposed for coronary artery bypass grafts in [12], and [13], respectively. However, cameras and endoscopes can only visualize the heart's outer surface and are not useful for procedures performed inside the heart such as valve repairs.

US images have been proposed for procedures performed inside the heart as they can visualize through the opaque blood pool. US images, however, present certain challenges. First,

Manuscript received: August, 27, 2015; Revised December, 19, 2015; Accepted January, 26, 2016.

This paper was recommended for publication by Editor Editor name upon evaluation of the Associate Editor and Reviewers' comments. *This work was supported by the Natural Sciences and Engineering Research Council (NSERC) of Canada RGPIN 03907 and RGPIN 372042, the Canada Foundation for Innovation (CFI) LOF 28241, an Alberta Innovation and Advanced Education Ministry Small Equipment Grant RCP-12-021, a University of Alberta Startup Grant, and a Queen Elizabeth II Graduate Student Scholarship from the Government of Alberta.

Meaghan Bowthorpe and Mahdi Tavakoli (corresponding author) are with the Department of Electrical and Computer Engineering, University of Alberta, AB, Canada. meaghan.bowthorpe@ualberta.ca, mahdi.tavakoli@ualberta.ca

they have a low frame rate, typically in the range of 20 to 60 Hz, compared to the heart motion's bandwidth. Second, they have a large image acquisition delay that is compounded by the subsequent image processing delay. Despite these added challenges, a motion compensating hand-held tool has been designed for mitral valve annuloplasty (MVA) under US guidance [14], [15], [16]. In this paper, we propose a control system for a motion compensating teleoperated surgical tool for use in intracardiac or extracardiac procedures performed under US guidance, which accounts for the master and slave robot dynamics not present with hand-held surgical tools.

The remainder of this paper is organized as follows. The challenges to overcome when designing the control system are discussed in Sec. II. The control algorithm, generalized predictive control, is discussed in Sec. III and is implemented in Sec. IV. Finally, a surgical task based on MVA and the conclusion are presented in Secs. V and VI, respectively.

II. Surgical Robot Control System

As discussed previously, it is too difficult for a surgeon to operate on a beating heart, but a surgical robotic system can assist the surgeon by compensating for the POI's motion. *The key is to control the distance between the surgical robot and the POI to follow the surgeon's motion.* This work will focus on image-based sensors, more specifically US images, as we propose a surgical system design for procedures performed inside or outside the heart. Because US images were chosen, the main issues to be addressed by the surgical robot feedback control system are:

1) *Delay in image data acquisition and processing*: If left uncompensated for, this delay may destabilize the surgical robot control loop, possibly resulting in collisions between the surgical robot and the POI.

2) *Slow sampling of image data*: The slowly sampled position measurements from the images must first be upsampled before being used in the surgical robot's feedback control loop to ensure a smooth response and to take advantage of the robot's faster sampling rate.

US imaging also suffers from artifacts. These include structures appearing in the wrong location, reverberation, speed displacement artifacts, and shadowing due to a strong attenuator [17]. This will be addressed in future work.

Previously, we have compensated for the delay within the feedback loop using a Smith predictor [18]. The Smith predictor, like many controllers, calculates the surgical robot's control signal based on the delayed and estimated current position errors, the error between the desired and actual robot position. It does not take any future position errors into account as the future output (actual position) and input (error between the robot's desired and actual position) values are unknown in most control applications. However, because the POI's motion is quasi-periodic, we can predict the POI's future positions, and hence know part of the robot's desired future position. In addition, with a model of the surgical robot, we can estimate its reaction to a control signal to estimate future outputs. As the input to the controller is the error between the desired position, the summation of the POI's and the surgeon's motion, and the surgical robot's actual motion and the output is the surgical robot's motion, estimates of the future input and output signals can be calculated, provided the surgeon can operate with a short delay in the transmission of his/her hand motions. Although it is more difficult, surgeons are able to perform a surgical procedure under teleoperation with delays of up to 300 ms [19]. Generalized predictive control (GPC) takes advantage of these estimated values and calculates the optimal control signal over a given horizon into the future.

We have previously presented two configurations of GPC for motion compensation in [20]. The first controlled the distance between the surgical tool tip and the POI to follow the surgeon's motion and treated the POI's motion as a disturbance. The second controlled the surgical tool to follow the summation of the POI's and surgeon's motion. The second method performed better as the POI's motion was not treated as a disturbance. In this paper, the surgical robot is controlled to follow the summation of the surgeon's and the POI's motion, but the control is performed at 100 Hz under US guidance with the help of a motion upsampler for smooth robot motions. Previously, it was performed at 20 Hz using a camera-based motion tracker [20]. The addition of this upsampler increases the image processing delay, making this challenge even harder to overcome. In addition, a user study involving a task based on MVA is presented to show the benefits of the motion compensation algorithm when performing a task on a moving POI.

III. Generalized Prediction Control

In GPC, the control signal is calculated by minimizing the difference between the estimated system output and the reference signal over a specified horizon while limiting the control signal [21]. Therefore, a model of the robot is required to estimate future outputs based on the current and future control signals.

To design a GPC law, we begin with a controlled auto-regressive integrated moving average (CARIMA) model to describe the robot dynamics:

$$A(z^{-1})y[kt] = B(z^{-1})u[(k-1)t]z^{-d} + \frac{C(z^{-1})}{\Delta}e[kt] \quad (1)$$

In the above, z^{-1} is the backward shift operator, $\Delta = 1 - z^{-1}$, t is the sampling interval, and k is an integer. The current system output is $y[kt]$, the previous sampling interval's control signal (input) is $u[(k-1)t]$, and the current disturbance is $e[kt]$. A, B, and C are polynomials of order n_a, n_b, and n_c respectively.

$$A(z^{-1}) = 1 + a_1 z^{-1} + a_2 z^{-1} + \ldots + a_{n_a} z^{-1} \quad (2a)$$

$$B(z^{-1}) = b_0 + b_1 z^{-1} + b_2 z^{-1} + \ldots + b_{n_b} z^{-1} \quad (2b)$$

$$C(z^{-1}) = 1 + c_1 z^{-1} + c_2 z^{-1} + \ldots + c_{n_c} z^{-1} \quad (2c)$$

The goal of GPC is to minimize the difference between the optimal prediction of the plant's future output positions given the current output position, i.e., $\hat{y}[(k+j)t|kt]$, and the future desired position values $w[(k+j)t]$ while keeping the change

in the control signal $\Delta u[(k+j-1)t]$ small. The cost function is then

$$J(N_1,N_2,N_u)=\sum_{j=1}^{N_u}\lambda(j)\Big[\Delta u[(k+j-1)t]\Big]^2+\sum_{j=N_1}^{N_2}\delta(j)\Big[\hat{y}[(k+j)t|kt]-w[(k+j)t]\Big]^2 \quad (3)$$

where N_1 and N_2 are the minimum and maximum costing horizons, N_u is the control horizon and is equal to N_1-N_2, and $\delta(j)$ and $\lambda(j)$ are weighting factors. To estimate future values of the output position $\hat{y}[(k+j)t]$, we start with the following Diophatine equation:

$$1=E_j(z^{-1})\tilde{A}(z^{-1})+z^{-j}F_j(z^{-1}) \quad (4)$$

where $\tilde{A}(z^{-1})=\Delta A(z^{-1})$, and $E_j(z^{-1})$ and $F_j(z^{-1})$ are polynomials of degree $j-1$ and n_a, respectively. $E_j(z^{-1})$ and $F_j(z^{-1})$ can be uniquely found given $A(z^{-1})$. Now multiplying (1) by $\Delta E_j(z^{-1})z^j$, considering (4), and the white noise case where $C(z^{-1})=1$, we obtain

$$\begin{aligned}\hat{y}[(k+j)t]&=F_j(z^{-1})y[kt]+E_j(z^{-1})e[(k+j)t]\\&+E_j(z^{-1})B(z^{-1})\Delta u[(k+j-d-1)t]\end{aligned} \quad (5)$$

Assuming the best estimate of future errors $e[(k+j)t]$ is 0,

$$\begin{aligned}&\hat{y}[(k+j)t|kt]=\\&F_j(z^{-1})y[kt]+G_j(z^{-1})\Delta u[(k+j-d-1)t]\end{aligned} \quad (6)$$

where $G_j(z^{-1})=E_j(z^{-1})B(z^{-1})$.

Separating the future and past changes in the control signal Δu, (6) can be rewritten in vector form as:

$$\mathbf{y}=\mathbf{Gu}+\mathbf{F}(z^{-1})y[kt]+\mathbf{G'}(z^{-1})\Delta u[(k-1)t]=\mathbf{Gu}+\mathbf{f} \quad (7)$$

where

$$\mathbf{y}=\begin{bmatrix}\hat{y}[(k+d+1)t|kt]\\\hat{y}[(k+d+2)t|kt]\\\vdots\\\hat{y}[(k+d+N_u)t|kt]\end{bmatrix} \quad (8)$$

$$\mathbf{G}=\begin{bmatrix}g_0&0&\dots&0\\g_1&g_0&\dots&0\\\vdots&\vdots&\vdots&\vdots\\g_{N_u-1}&g_{N_u-2}&\dots&g_0\end{bmatrix} \quad (9)$$

$g_0,g_1,\dots,g_{N_u-1}$ are the coefficients of G_j,

$$\mathbf{u}=\begin{bmatrix}\Delta u[kt]\\\Delta u[(k+1)t]\\\vdots\\\Delta u[(k+N_u-1)t]\end{bmatrix} \quad (10)$$

$$\mathbf{G'}(z^{-1})=\begin{bmatrix}(G_{d+1}(z^{-1})-g_0)z\\(G_{d+2}(z^{-1})-g_0-g_1z^{-1})z^2\\\vdots\\(G_{d+N_u}(z^{-1})-g_0-g_1z^{-1}-\dots g_{N_u-1}z^{N_u-1})z^N\end{bmatrix} \quad (11)$$

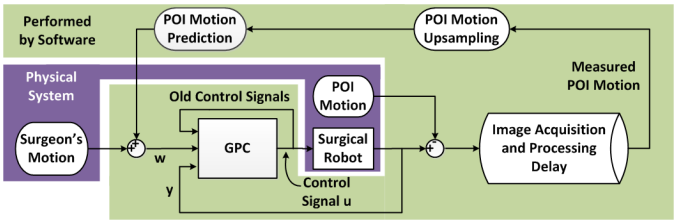

Fig. 1: The robot-assisted beating-heart surgical system where the surgical tool tip is controlled to follow the summation of the surgeon's and the estimated POI motion, which is calculated from the POI's motion in the previous heart beat.

and

$$\mathbf{F}(z^{-1})=\begin{bmatrix}F_{d+1}(z^{-1})\\F_{d+2}(z^{-1})\\\vdots\\F_{d+N_u}(z^{-1})\end{bmatrix} \quad (12)$$

The cost function can be rewritten in vector form as

$$J=(\mathbf{Gu}+\mathbf{f}-\mathbf{w})^T(\mathbf{Gu}+\mathbf{f}-\mathbf{w})+\lambda\mathbf{u}^T\mathbf{u} \quad (13)$$

where

$$\mathbf{w}=\begin{bmatrix}w[(k+1)t]\\\vdots\\w[(k+N_u)t]\end{bmatrix} \quad (14)$$

From (13), $\Delta u[kt]$ can be calculated as:

$$\Delta u[kt]=K(\mathbf{w}-\mathbf{f}) \quad (15)$$

where $\mathbf{K}=(\mathbf{G}^T\mathbf{G}+\lambda\mathbf{I})^{-1}\mathbf{G}^T$, I is an identity matrix with the same size as $\mathbf{G}$, λ is a weighting factor, and K is the first row of $\mathbf{K}$. For more details see [22].

IV. Surgical Robot Control Algorithm

The controller is shown in Fig. 1. The reference signal w is the summation of the surgeon's and the estimated POI motion and the output y is the surgical tool's position. In the figure, the darker section is the physical system that cannot be changed and the lighter section is performed by software and can be changed. To run this controller at 100 Hz, the POI's motion is upsampled and predicted the length of the horizon into the future to overcome the total delay caused by the US image acquisition, processing, and upsampling.

A. Heart Motion Measurement

The image processing presented in this paper to locate the POI does not require any markers and is completed within one sample time at the image acquisition rate of 34 Hz. The image processing is summarized in Fig. 2.

Initially, a binary threshold is applied to convert the gray-scale images to black and white. First, the surgical tool is found as it points to the POI's location. A Hough transform finds the longest straight line that forms an angle with the horizontal within a $\frac{\pi}{4}$ radians angular arc – the surgical tool's expected location – in the first image. To reduce the processing time of the remaining images, a region of interest (ROI) is

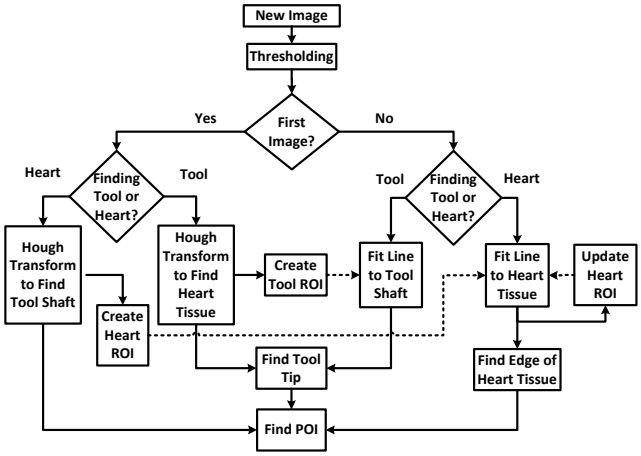

Fig. 2: The image processing algorithm. Each image is thresholded to create a black and white image. Hough transforms locate the tool shaft and heart tissue in the first image. The ROIs are set and the tool tip and POI locations are found. Lines are fit to the tool shaft and heart tissue, the edge of the heart tissue is found, the heart tissue ROI is updated, and the tool tip and POI locations are found.

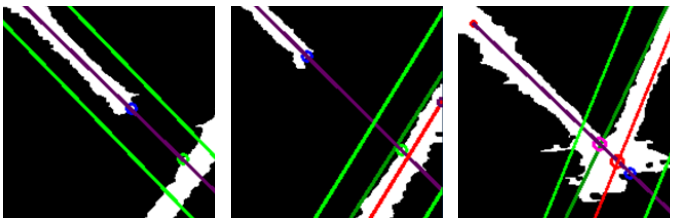

(a) (b) (c)

Fig. 3: The processed images showing the surgical tool shaft and tip (a) and the heart tissue and POI (b) and (c). The light green lines mark the ROIs, the purple line shows the surgical tool shaft, the blue dot shows the surgical tool tip in (a) and (b), the green dot shows the POI in (b), and the pink dot shows the surgical tool tip and POI in (c).

created surrounding the surgical tool. In the remaining images, least squares regression by OpenCV's fitline() identifies the centre line of the surgical tool's shaft [23]. To lessen the computational burden, the ROI is down-sampled and only every third column and row of the ROI are analysed for candidate pixels. Fig. 3a shows the result of finding the tool. The green lines mark the ROI surrounding the tool shaft, the purple line marks the center line of the tool shaft, and the blue dot marks the tool tip.

The heart tissue is found in a similar manner. In the first image, a Hough transform identifies the longest line within a $\frac{\pi}{4}$ radians angular arc perpendicular to the surgical tool shaft. A second ROI is created surrounding the heart tissue. In all subsequent images, the heart tissue is identified using OpenCv's fitline(). Once again, to reduce the computation time, the image is down-sampled and only every third column and row are analysed for candidate pixels. Within every subsequent image, the candidate pixels on the closest edge of the heart tissue to the tool are identified and a straight line is fit through them to locate the edge of the heart tissue. As the heart tissue moves continually, the heart tissue ROI is updated with every image. Figs. 3b and 3c show the result of finding the heart tissue when the surgical tool and the heart tissue are not and are in contact, respectively. The heart tissue ROI is marked by the light green lines, the dark green line marks the edge of the heart tissue, and the red line marks the centre line of the heart tissue.

The POI's location is found by extending the line through the surgical tool shaft and locating the first candidate pixel beyond the surgical tool's tip – the heart tissue. However, a difficulty arises when the surgical tool tip makes contact with the heart tissue. In this case, it is not possible to identify the surgical tool's tip as the surgical tool and the heart tissue appear as one object. When the surgical tool is touching the heart tissue, i.e., when the line marking the surgical tool tip intersects with the line marking the heart tissue, the POI is identified by the intersection of the line marking the edge of the heart tissue and the line through the surgical tool shaft. The POI's location when the surgical tool and the heart do not touch is the green dot in Fig. 3b and when they do touch the POI is the pink dot in Fig. 3c.

B. Heart Motion Upsampling

After the POI's motion is measured from the US images, it is upsampled using cubic interpolation, which ensures that the upsampled trajectory and its first derivative are smooth. Consider the data points p_0 and p_1, in between which the interpolation is to occur. One data point before p_0 and one data point after p_1 are required to calculate the slope at p_0 and at p_1. Consequently, four data points, two of which are in the future with respect to the interval being interpolated, are required, which increases the time delay by the length of two samples at the slow sampling rate.

The following calculates the interpolated data points:

$$p(n) = h_{00}(n)p_0 + h_{10}(n)m_0 + h_{01}(n)p_1 + h_{11}(n)m_1 \quad (16)$$

where m_0 and m_1 are the slopes at points p_0 and p_1, respectively, and n is the interpolation variable, which is a vector with a length of one greater than the number of points to be interpolated and with evenly spaced values ranging from 0 and 1. When n equals 0 and 1, the result is p_0 and p_1, respectively. The h coefficients are:

$$\begin{aligned} h_{00}(n) &= 2n^3 - 3n^2 + 1 \\ h_{10}(n) &= n^3 - 2n^2 + n \\ h_{01}(n) &= -2n^3 + 3n^2 \\ h_{11}(n) &= n^3 - n^2 \end{aligned} \quad (17)$$

C. Heart Motion Prediction

Another issue to overcome is the non-negligible delay in acquiring, processing, and upsampling the POI's position. To address this, the POI's motion is modeled as a Fourier series and an extended Kalman filter predicts its future motion.

$$y(\mathbf{x}(t)) = c + \sum_{i=1}^{m} r_i \sin\theta_i(t) \tag{18}$$

In the above, $\theta_i(t) = i\int_0^t \omega(\tau)d\tau + \phi_i(t)$, the state vector is defined as $\mathbf{x}(t) = [c(t), r_i(t), \omega(t), \theta_i(t)]^T$, $i = 1, \ldots, m$, m is the number of harmonics, and t is the current time. The coefficients in (18) can vary with time to account for cycle-to-cycle heart motion variation [16].

The state space model (19) evolves through random walk, where the offset c, the sine wave coefficients, r_l, and the frequency ω are assumed to remain constant. These values are then updated by the EKF proportionally to the error between the predicted and actual measurement, except for the frequency, ω, which is replaced by the value measured directly from the past POI motion.

$$\begin{aligned} \mathbf{x}(t+\Delta t) &= \mathbf{L}(\Delta t)\mathbf{x}(t) + \mu(t) \\ z(t) &= y(\mathbf{x}(t)) + \upsilon(t) \end{aligned} \tag{19}$$

Here, $\mathbf{L}(\Delta t)$ is a $[2m+2] \times [2m+2]$ matrix:

$$\mathbf{L}(\Delta t) = \left[\begin{array}{c|ccccc} \mathbf{I}_{m+1} & & & 0 & & \\ \hline & 1 & & & & \\ & \Delta t & 1 & & & \\ \mathbf{0} & 2\Delta t & 0 & 1 & & \\ & \vdots & & & \ddots & \\ & m\Delta t & & & & 1 \end{array}\right] \tag{20}$$

The estimated covariance matrix $\mathbf{P}(t + \Delta t|t)$ is a $[2m + 2] \times [2m + 2]$ diagonal matrix with $[0.001, 0.1/1, 0.1/2, ..., 0.1/l, 0.1, 0.2_{1\times m}]$ along the diagonal, the process noise covariance matrix $\mathbf{Q}$ is a $[2m+2]\times[2m+2]$ diagonal matrix with 0.0001 along the diagonal, and the observation noise covariance matrix σ_R^2 is 0.01. The Kalman gain $\mathbf{K}$ and $\mathbf{P}(t + \Delta t|t)$ are calculated as:

$$\mathbf{P}(t+\Delta t|t) = \mathbf{L}(\Delta t)\mathbf{P}(t|t)\mathbf{L}(\Delta t)^T + \mathbf{Q} \tag{21a}$$

$$S = \sigma_R^2 + \mathbf{H}\mathbf{P}(t+\Delta t|t)\mathbf{H}^T \tag{21b}$$

$$\mathbf{K} = \mathbf{P}(t+\Delta t|t)\mathbf{H}^T S^{-1} \tag{21c}$$

The state and covariance matrices are updated as follows:

$$\begin{aligned} \hat{\mathbf{x}}(t+\Delta t|t+\Delta t) =& \mathbf{L}(\Delta t)\hat{x}(t|t) \\ &+ \mathbf{K}(z(t+\Delta t) - h(\mathbf{L}(\Delta t)\hat{\mathbf{x}}(t|t))) \end{aligned} \tag{22a}$$

$$\mathbf{P}(t+\Delta t|t+\Delta t) = (\mathbf{I} - \mathbf{K}\mathbf{H})\mathbf{P}(t+|\Delta t|t) \tag{22b}$$

In the above, $\mathbf{H}$ is a $[2m+2]\times[1]$ matrix:

$$\begin{aligned} \mathbf{H}^T(\Delta t) &= \left(\frac{\partial h}{\partial \mathbf{x}}\right)^T \Bigg|_{\hat{\mathbf{x}}(t+\Delta t|t)=\mathbf{L}\hat{\mathbf{x}}(t|t)} \\ &= \begin{bmatrix} 1 \\ \sin\hat{\theta}_1(t+\Delta t|t) \\ \vdots \\ \sin\hat{\theta}_m(t+\Delta|t) \\ 0 \\ \hat{r}_1(\Delta t|t)\cos\hat{\theta}_1(t+\Delta t|t) \\ \vdots \\ \hat{r}_m(\Delta t|t)\cos\hat{\theta}_m(t+\Delta t|t) \end{bmatrix} \end{aligned} \tag{23}$$

To predict j future points ahead, the estimated state matrix $\hat{\mathbf{x}}$ is multiplied by the update matrix $\mathbf{L}\Delta(t)$ a total of j times, $\hat{\mathbf{x}}(t+j\Delta t|t+\Delta t) = \mathbf{L}^j\hat{\mathbf{x}}(t+\Delta t|t)$. The predicted position is then calculated from the predicted state and (18).

With this upsampled and predicted POI motion, the surgical robot can be controlled with GPC to follow the surgeon's motions and synchronize with the POI's motions. This will allow the surgeon to operate on a seeminly stationary heart, even though it is actually beating. Note, this system is designed for one-dimensional motion tracking under US guidance. This is sufficient for procedures such as MVA (described in more detail in Sec. V-A) or tissue palpation. The mitral valve's motion was measured in [14] and was shown be primarily along a single axis. The system is now tested to determine its effectivenss for a user operating on a moving POI.

V. Experimental Results

The experimental setup shown in Fig. 4 uses a 6 MHz 4DL14-5/38 linear 4D transducer connected to a SonixTouch US scanner (SonixTouch from Ultrasonix, Richmond, BC, Canada) as the image sensor, which has a low frame rate of 34 Hz. The depth of the images was 4.5 cm. The 2D US images were collected from the US scanner using a DVI2USB 3.0 frame grabber (Epiphan, Ottawa, ON, Canada). The entire image acquisition, processing and upsampling delay is 170 ms. A custom-built mechanical cam (simulated heart), based on the motion collected from the movement of a point on the side wall of the heart in a series of clinical US images of a patient's beating heart generated the POI motion. The single degree-of-freedom (DOF) surgical tool (surgical robot) is actuated by a voice coil motor (NCC20-18-020-1X from H2W Technologies Inc., Santa Clarita, CA, USA). The surgical tool is described in more detail in [24]. To verify the results, real-time position measurements of both the mechanical cam and the robot were collected from two potentiometers (LP-75FP-5K and LP-30FP-1K from Midori America Corp., Fullerton, CA, USA).

To implement the GPC system, an electromechanical model of the surgical robot composed of the voice coil actuator and the corresponding analog current drive circuitry is identified. The voice coil actuator was modeled as in [25] where the relationship between the input current, I, and the position, θ of the voice coil actuator is

$$I = \left(\frac{1}{sL+R}\right)\left(\frac{K_t}{sJ+B}\right)\left(\frac{1}{s}\right)\theta \tag{24}$$

The inductance L and resistance R of the voice coil are 1.05 mH and 3.5 Ω, respectively, and the back EMF gain K_t is 6.1 V/m. The parameters J and B were found to be -0.5264 and 16.2547 using least squares identification. Discretized to 100 ms, the robot's transfer function between the input current and the output position is given in (25). The weighting factors $\lambda(j)$ and $\delta(j)$ were set to 0.00003 and 1, respectively. The delay, d was 2 samples and the control horizon, N_u, was 5 samples.

For each trial, the heartbeat motion has a peak-to-peak amplitude of 10 mm and a period of 64 bpm (1.07 Hz). Three error metrics are calculated for each trial: the mean absolute error (MAE) is $\frac{\sum|error|}{l}$, where l is the number of data points

$$I = \frac{-6.764 \times 10^{-5} - 0.0002029z^{-1} - 0.0002029z^{-2} - 6.764 \times 10^{-5}z^{-3}}{1 - 0.8457z^{-1} - 0.8039z^{-2} + 0.6469z^{-3}}\theta \tag{17}$$

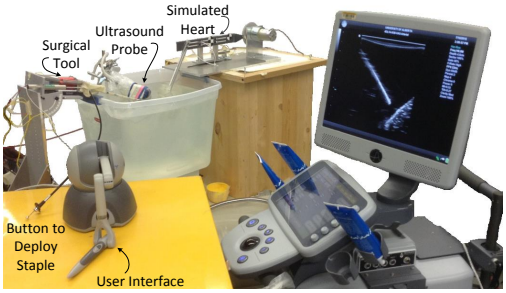

Fig. 4: The experimental setup.

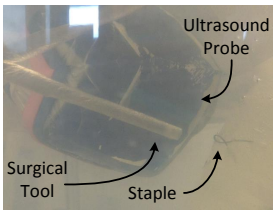

(a)

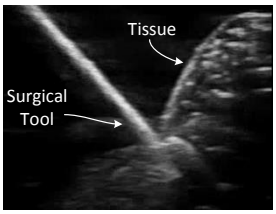

(b)

Fig. 5: The surgical task based on MVA where the user deploys a staple.

in the sample, the integral squared error (ISE) is $\frac{\sum(error)^2}{l}$, and the peak tracking error (PTE) is the largest error at a single point in time. The results are summarized in Table I.

A. Surgical Task

When the mitral valve is not shaped properly, blood may flow backwards through the heart making each beat less efficient. More than 300,000 people undergo MVA – a reconstructive procedure to fix the leaky valve – each year worldwide [26]. The surgical task presented here simulates deploying a staple to secure an annuloplasty ring onto the mitral valve. If securing this annuloplasty ring could be performed while the heart is still beating, the effectiveness of the newly reshaped valve could be evaluated immediately. This user study was approved by the University of Alberta's Research Ethics Office #Pro00055825.

In this user study, each participant deploys the staple into moving heart tissue. The participant sets the desired position of the surgical tool through teleoperation by moving the stylus of a PHANToM Omni user interface (Geomagic, Cary, NC, USA). The heart tissue is represented by a piece of soft plastic visible under US and is mounted on the mechanical cam, which is the simulated beating heart. The participant views the scene on the US screen. The participant holds a button in his or her other hand and presses this button to deploy the staple. A successfully deployed staple is shown in Fig. 5a.

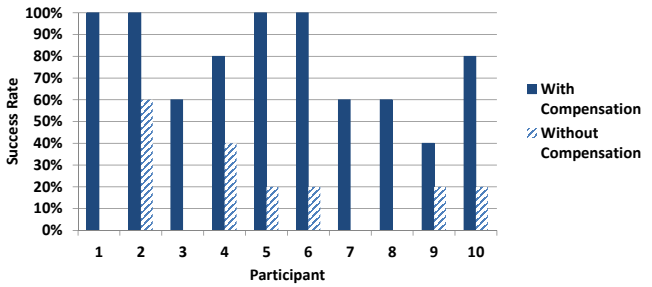

Fig. 6: The rate of successful staple deployment by participant.

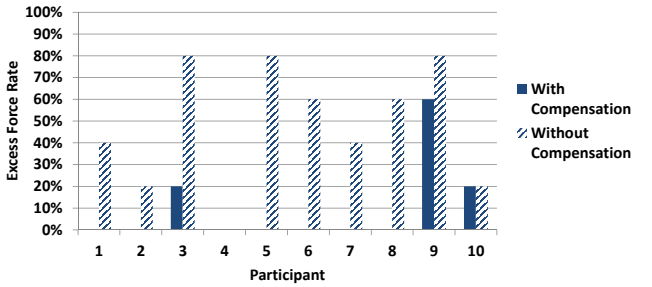

Fig. 7: The rate of the use of excessive force by participant.

The participants attempt to complete this task with and without motion compensation. For these trials, the heart motion was divided into two halves - the upper half where the heart tissue was closest to the surgical tool and the lower half where it was furthest away – this was where the participant was told to deploy the staple. This prevented the participant from simply waiting until the heart came towards the surgical tool to deploy the staple as this would have made the task too easy and not representative of real surgical maneuvers. Each participant was also instructed not to press the tool into the tissue when deploying the staple.

Each participant's pre-trial training included successfully deploying the staple three times with motion compensation. They then practiced with no compensation until they felt comfortable with the system. Each participant completed 10 trials; 5 with motion compensation and 5 without. The trials alternated between the two conditions beginning with motion compensation. If the surgical tool left an indent in the phantom tissue when the staple was deployed or if the staple was deployed in the upper half of the heart beat when the surgical tool was closest to the hear (see Fig. 5b), the trial was counted as a failure.

The trials included 10 participants (2 females and 8 males), who were not surgeons. Without motion compensation, the staple was successfully deployed in 18% of the trials and

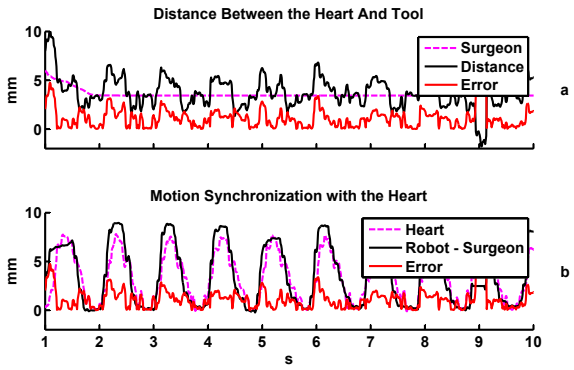

Fig. 8: The result when motion compensation is provided. In case (a), the dashed pink line is the user's motion, the solid black line is the distance between the surgical tool tip and the heart tissue, and the red line is the error between these two. Case (b) shows the motion synchronization. Here, the surgeon's motions have been subtracted from the surgical tool tip's motion leaving the POI following portion of the surgical tool tip's motion – the solid black line. The heart's motion is the dotted pink line and the error between the two is the red line.

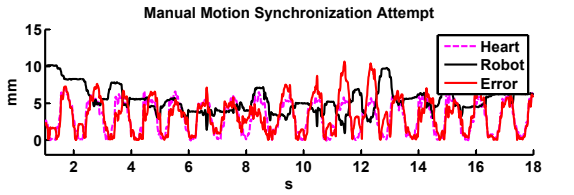

Fig. 9: The result when no motion compensation is provided. Here the user tries to manually compensate for the heart's motion. The surgical tool tip's motion is the solid black line, the heart's motion is the dotted pink line and the error between the two is the red line.

excessive force was used in 48% of the trials. With motion compensation, the success rate was 78% and the use of excessive force was reduced to 10% of the trials. The success rate of each participant is given in Fig. 6 and the rate of the use of excessive force is given in Fig. 7.

To compare the success rates, we used a two-tailed *t-test* and obtained the probability of the null hypothesis $\mu_1 = \mu_2$ for the 10 trials [27]. The probability of the results assuming the null hypothesis for the success of the staple deployment and the use of excess force with and without compensation was 2×10^{-5} and 0.002, respectively. Since these figures are less than 0.05, they indicate that there was a significant difference between providing and not providing motion compensation with respect to both the successful deployment of the staple and the use of excessive force.

Now, as a final metric, let us evaluate the system performance by examing the position synchornization errors. We will take a closer look at the position tracking errors and how much

Motion Compensation	MAE (mm)	ISE (mm^2)	PTE (mm)
Yes	1.27	3.17	7.18
No	3.03	15.59	10.16

TABLE I: A summary of the experimental results

the users were required to move when performing the surgical task. When motion compensation was provided, it was easier for the user to move the surgical tool towards the moving heart tissue. The user's motions for this case creates the pink line in Fig. 8a. The user's motion simply moves the surgical tool tip towards the heart tissue. The solid black line in this figure is the resulting distance between the surgical tool tip and the POI and the solid red line is the error. In Fig. 8b the surgeon's motion has been subtracted from the surgical tool tip's motion to remove the offset between the surgical tool tip motion and the POI motion – the solid black line – to show the motion synchronization. The POI's motion is the dashed pink line and the error is the solid red line. The MAE tracking error when motion compensation is provided is 1.27 mm, the ISE tracking error is 3.17 mm^2, and the absolute value of the PTE is 7.18 mm.

It is much harder for the user to follow the POI's motion when no motion compensation is provided. Fig. 9 shows the surgeon's motion – the solid black line and the POI's motion – the dashed pink line. It is quite obvious that the errors are quite large – the solid red line. The MAE tracking error when motion compensation is not provided is 3.03 mm, the ISE tracking error is 15.59 mm^2, and the absolute value of the PTE is 10.16 mm. A video showing the results of this user task is available from the IEEE website.

The average tracking error reported in this work, 1.27 mm, is similar to those reported in the literature. It is difficult to make a fair comparison of errors, because many systems proposed in the literature do not deal with such slow sample rates and such large time delays. Sub-millimetre errors were reported when a 500 Hz camera measured the POI's position and the time delay was limited to one sample time in [13]. The use of pre-recorded data resulted in average errors as low as 0.669 mm and PE as large as 4.3 mm in [8]. However, this method is not viable in real-time. The use of motion compensation after the heart is stabilized by a mechanical stabilizer resulted in small errors of 0.4 and 0.8 mm in the x and y directions and a PTE of 2 mm in the y-direction in [1]. However, this method does not let the heart beat freely. Finally, an average and PTE of 0.97 mm and 3.26 mm respectively was reported in [16] where the POI motion was measured from US images. A similar user task performed with a hand-held motion compensating surgical tool reported a success rate of 74% when motion compensation was provided and only 32% when motion compensation was not provided [28].

VI. Conclusion

This paper presents an image processing and control system for US-guided robot-assisted beating heart surgery for procedures such as MVA. As the heart's position is measured from US images that are collected at a slow sampling rate, the POI's

motion is first upsampled to 100 Hz. To overcome the time delay caused by US image acquisition and processing as well as motion upsampling, the POI motion trajectory is predicted ahead to the current time using an EKF. Generalized predictive control is used to optimally compensate for the heart's current and future beating motion. To show the efficacy of this system, user trials simulating deploying a staple for MVA were conducted. The results indicate that the improvement in the success rate and reduction in use of excessive force when motion compensation is provided is statistically significant.

REFERENCES

[1] T. Ortmaier, M. Groger, D. H. Boehm, V. Falk, and G. Hirzinger, "Motion estimation in beating heart surgery," *IEEE Trans. on Biomedical Engineering*, vol. 52, no. 10, pp. 1729–1740, 2005.

[2] G. Reed, D. Singer, E. Picard, and R. DeSanctis, "Stroke following coronary-artery bypass surgery. a case-control estimate of the risk from carotid bruits," *The New England Journal of Medicine*, vol. 319, pp. 1246–1250, 1988.

[3] M. F. Newman, J. L. Kirchner, B. Phillips-Bute, V. Gaver, H. Grocott, R. H. Jones, D. B. Mark, J. G. Reves, and J. A. Blumenthal, "Longitudinal assessment of neurocognitive function after coronary-artery bypass surgery," *New England Journal of Medicine*, vol. 344, no. 6, pp. 395–402, 02/08 2001.

[4] B. Cagneau, N. Zemiti, D. Bellot, and G. Morel, "Physiological motion compensation in robotized surgery using force feedback control," in *IEEE Int. Conf. on Robotics and Automation*, 2007, pp. 1881–1886.

[5] M. Dominici and R. Cortesao, "Model predictive control architectures with force feedback for robotic-assisted beating heart surgery," in *IEEE Int. Conf. on Robotics and Automation*, 2014, In Press.

[6] S. Kesner and R. Howe, "Discriminating tissue stiffness with a haptic catheter: Feeling the inside of the beating heart," in *IEEE World Haptics Conference*, June 2011, pp. 13–18.

[7] ——, "Motion compensated catheter ablation of the beating heart using image guidance and force control," in *Int. Symposium on Experimental Robotics*, 2012.

[8] O. Bebek and M. C. Cavusoglu, "Intelligent control algorithms for robotic-assisted beating heart surgery," *IEEE Trans. on Robotics*, vol. 23, no. 3, pp. 468–480, 2007.

[9] E. Tuna, T. Franke, O. Bebek, A. Shiose, K. Fukamachi, and M. Cavusoglu, "Heart motion prediction based on adaptive estimation algorithms for robotic-assisted beating heart surgery," *IEEE Trans. on Robotics*, vol. 29, no. 1, pp. 261–276, 2013.

[10] J. Rotella, "Predictive tracking of quasi periodic signals for active relative motion cancellation in robotic assisted coronary artery bypass graft surgery," Master's thesis, Case Western Reserve University, January 2005.

[11] T. Horiuchi, E. Tuna, K. Masamune, and M. Cavusoglu, "Heart motion measurement with three dimensional sonomicrometry and acceleration sensing," in *IEEE/RSJ Int. Conf. on Intelligent Robots and Systems*, 2012, pp. 4143–4149.

[12] Y. Nakamura, K. Kishi, and H. Kawakami, "Heartbeat synchronization for robotic cardiac surgery," in *IEEE Int. Conf. on Robotics and Automation*, vol. 2, 2001, pp. 2014–2019 vol.2.

[13] R. Ginhoux, J. Gangloff, M. de Mathelin, L. Soler, M. M. A. Sanchez, and J. Marescaux, "Active filtering of physiological motion in robotized surgery using predictive control," *IEEE Trans. on Robotics*, vol. 21, no. 1, p. 67, 2005.

[14] D. T. Kettler, R. D. Plowes, P. M. Novotny, N. V. Vasilyev, P. J. del Nido, and R. D. Howe, "An active motion compensation instrument for beating heart mitral valve surgery," in *IEEE/RSJ Int. Conf. on Intelligent Robots and Systems*, 2007, pp. 1290–1295.

[15] P. M. Novotny, J. A. Stoll, P. E. Dupont, and R. D. Howe, "Real-time visual servoing of a robot using three-dimensional ultrasound," in *IEEE Int. Conf. on Robotics and Automation*, 2007, pp. 2655–2660.

[16] S. G. Yuen, P. M. Novotny, and R. D. Howe, "Quasiperiodic predictive filtering for robot-assisted beating heart surgery," in *IEEE Int. Conf. on Robotics and Automation*, 2008, pp. 3875–3880.

[17] M. Feldman, S. Katyal, and M. Blackwood, "US artifacts," *RadioGraphics*, vol. 29, pp. 1179–1189, 2009.

[18] M. Bowthorpe, M. Tavakoli, , H. Becher, and R. Howe, "Smith predictor based robot control ultrasound-guided teleoperated beating-heart surgery," *IEEE Journal of Biomedical and Health Informatics*, vol. 18, no. 1, pp. 157–166, 2013.

[19] R. Rayman, S. Primak, R. Patel, M. Moallem, R. Morady, M. Tavakoli, V. Subotic, N. Galbraith, A. van Wynsberghe, and K. Croome, *Effects of Latency on Telesurgery: An Experimental Study*, ser. Medical Image Computing and Computer-Assisted Intervention. Springer Berlin / Heidelberg, 2005, vol. 3750, pp. 57–64.

[20] M. Bowthorpe, A. Alvarez Garcia, and M. Tavakoli, "Gpc-based teleoperation for delay compensation and disturbance rejection in image-guided beating-heart surgery," in *IEEE Int. Conf. on Robotics and Automation*, May 2014, pp. 4875–4880.

[21] D. Clarke, C. Mohtadi, and P. Tuffs, "Generalized predictive control part i. the basic algorithm," *Automatica*, vol. 23, no. 2, pp. 137 – 148, 1987.

[22] E. F. Camacho and C. Bordons, *Model Predictive Control*, M. J. Grimble and M. A. Johnson, Eds. Springer, 1999.

[23] "Opencv library: http://opencv.org."

[24] M. Bowthorpe, V. Castonguay-Siu, and M. Tavakoli, "Development of a robotic system to enable beating-heart surgery," *Jour. of the Robotics Society of Japan, invited paper*, vol. 32, no. 4, pp. 339–346, 2014.

[25] R. Oboe, F. Marcassa, and G. Maiocchi, "Hard disk drive with voltage-driven voice coil motor and model-based control," *IEEE Trans. on Magnetics*, vol. 41, no. 2, pp. 784–790, 2005.

[26] M. Rausch, W. Bothe, J. Kvitting, J. Swanson, D. Miller, and E. Kuhl, "Mitral valve annuloplasty," *Annals of Biomedical Engineering*, vol. 40, no. 3, pp. 750–761, 2012.

[27] G. Snedecor and W. Cochran, *The Two-tailed T-Test*. The Iowa State University Press, 1967, pp. 59–60.

[28] S. Yuen, S. Kesner, N. Vasilyev, P. Del Nido, and R. Howe, "3D ultrasound-guided motion compensation system for beating heart mitral valve repair," in *Medical Image Computing and Computer-Assisted Intervention*, ser. Lecture Notes in Computer Science. Springer Berlin / Heidelberg, 2008, vol. 5241, pp. 711–719.